

Pressure shifts and abundance gradients in the atmosphere of the DAZ white dwarf GALEX J193156.8+011745 ^{*}

S. Vennes^{1†}, A. Kawka^{1†}, and P. Németh^{1,2†}

¹*Astronomický ústav AV ČR, Fričova 298, CZ-251 65 Ondřejov, Czech Republic*

²*Department of Physics and Space Sciences, 150 W. University Blvd, Florida Institute of Technology, Melbourne, FL 32901, USA*

ABSTRACT

We present a detailed model atmosphere analysis of high-dispersion and high signal-to-noise ratio spectra of the heavily polluted DAZ white dwarf GALEX J1931+0117. The spectra obtained with the VLT-Kueyen/UV-Visual Echelle Spectrograph show several well-resolved Si II spectral lines enabling a study of pressure effects on line profiles. We observed large Stark shifts in silicon lines in agreement with theoretical predictions and laboratory measurements. Taking into account Stark shifts in the calculation of synthetic spectra we reduced the scatter in individual line radial velocity measurements from ~ 3 to $\lesssim 1$ km s⁻¹. We present revised abundances of O, Mg, Si, Ca, and Fe based on a critical review of line broadening parameters and oscillator strengths. The new measurements are generally in agreement with our previous analysis with the exception of magnesium with a revised abundance a factor of two lower than previously estimated. The magnesium, silicon and iron abundances exceed solar abundances, but the oxygen and calcium abundances are below solar. Also, we compared the observed line profiles to synthetic spectra computed with variable accretion rates and vertical abundance distributions assuming diffusive steady-state. The inferred accretion rates vary from $\dot{M} = 2 \times 10^6$ for calcium to 2×10^9 g s⁻¹ for oxygen. We find that the accretion flow must be oxygen-rich while being deficient in calcium relative to solar abundances. The lack of radial velocity variations between two measurement epochs suggests that GALEX J1931+0117 is probably not in a close binary and that the source of the accreted material resides in a debris disc.

Key words: stars: abundance – stars: individual: GALEX J193156.8+011745 – white dwarfs

1 INTRODUCTION

GALEX J193156.8+011745 (GALEX J1931+0117, thereafter) is a hydrogen-rich white dwarf discovered by Vennes, Kawka, & Németh (2010a) and characterized by an opulent heavy-element line spectrum and an infrared excess. The original low-resolution spectrum obtained with the New Technology Telescope (NTT) at La Silla Observatory showed a strong Mg $\lambda\lambda 4481$ doublet and weaker silicon lines. Follow-up echelle spectroscopy obtained with the Very Large Telescope (VLT)-Kueyen enabled a detailed abundance study. The near-solar abundances of oxygen, magnesium, silicon, calcium and iron bear the signature of an external supply of material accreting onto the surface of the white dwarf. Based on available data, Vennes et al. concluded that

the supply may originate from a close, sub-stellar companion or from a cool debris disc.

The presence of heavy elements in hydrogen-rich white dwarfs has variously been interpreted as intrinsic to the white dwarf, or as extrinsic, i.e., supplied by the interstellar medium (Dupuis, Fontaine, & Wesemael 1993), by a nearby companion as in post-common envelope systems (Debes 2006; Kawka et al. 2008), or by a debris disc (Zuckerman et al. 2003; Kilic et al. 2006; Farihi, Zuckerman, & Becklin 2008). However, accretion from the interstellar medium is unlikely because of supply shortages (Farihi et al. 2010a). In the extrinsic scenarios, the elements are accreted and diffused in the atmosphere and envelope of the star (see Fontaine & Michaud 1979; Koester 2009). An intrinsic, or internal, reservoir of heavy elements is also possible, but in either scenario a self-consistent solution of the diffusion equation must explore the effect of radiative acceleration on trace elements (Chayer, Fontaine, & Wesemael 1995; Chayer et al. 1995).

As a class, the polluted DA white dwarfs, or DAZs,

^{*} Based on observations made with ESO telescopes at the La Silla Paranal Observatory under programme 283.D-5060.

[†] E-mail: vennes@sunstel.asu.cas.cz (SV); kawka@sunstel.asu.cas.cz (AK); nemeth@sunstel.asu.cas.cz (NM)

are often defined by the detection of the Ca II H&K doublet in optical spectra of cooler objects (Zuckerman et al. 2003; Koester et al. 2005), or by the detection of carbon and silicon in the ultraviolet spectra of warmer objects (Dupuis et al. 2009a,b). Exceptionally, Mg II $\lambda 4481$ is, so far, only detected in a handful of warm white dwarfs such as EG 102 (Holberg, Barstow, & Green 1997), GALEX J1931+0117, and two warm white dwarfs from the Sloan Digital Sky Survey (SDSS) that show evidence of dusty and gaseous discs (Gänsicke et al. 2006; Gänsicke, Marsh, & Southworth 2007). The presence of a large concentration of magnesium in the last two objects helped establish a strong link between heavy element pollution and dense circumstellar environments. Moreover, an infrared excess that cannot otherwise be explained by a cool companion, may be attributed to a dust ring as in the case of the white dwarf G29-38 (Graham et al. 1990).

We present new high-dispersion spectroscopic observations that help elucidate the nature of the peculiar abundance pattern in GALEX J1931+0117 in support of the debris disc model. Our observations are presented in Section 2, and a detailed line profile and abundance analysis is presented in Section 3. In Section 3.1 we compile and evaluate line broadening parameters and oscillator strengths. In Section 3.2 we describe steady-state diffusion models and predicted abundance gradients in the stable atmospheres of hot white dwarfs. In Section 3.3 we present revised abundances based on a review of atomic data, we assess non-local thermodynamic equilibrium (non-LTE) effects on measured abundances, and we constrain the accretion rates on the atmosphere of GALEX J1931+0117. Finally, we conclude in Section 4.

2 OBSERVATIONS

Following the identification of GALEX J1931+0117 as a DAZ white dwarf we obtained a series of echelle spectra using standard settings with the UV-Visual Echelle Spectrograph (UVES) attached to the VLT-Kueyen. All spectra were obtained with the slit width set at $1''$, offering a resolving power $R \approx 46000$. The exposure times were 1450 s. The first series of spectra were obtained on UT 2009 Nov 12 (epoch 1, thereafter) with the dichroic #2 and the “HER_5” and “BK7_5” filters on the blue and red arms, respectively. The blue spectrum was centred at 4370\AA and covered the range $3757\text{--}4985\text{\AA}$, and the red spectra were centred at 7600\AA and covered the ranges $5698\text{--}7532$ and $7660\text{--}9464\text{\AA}$. The first series of spectra were analysed by us (Vennes, Kawka, & Németh 2010a). The second series of spectra were obtained on UT 2010 Mar 15 (epoch 2, thereafter) with the dichroic #1 and the “HER_5” and “SHP700” filters on the blue and red arms, respectively. The blue spectrum was centred at 3900\AA and covered the range $3290\text{--}4518\text{\AA}$, and the red spectra were centred at 5800\AA and covered the ranges $4788\text{--}5750$ and $5839\text{--}6808\text{\AA}$.

We remeasured the H α radial velocity by fitting Gaussian profiles to the well-exposed, narrow line cores obtained at epochs 1 and 2, $v_{\text{H}\alpha,1} = 37.6 \pm 0.8 \text{ km s}^{-1}$ and $v_{\text{H}\alpha,2} = 36.8 \pm 1.0 \text{ km s}^{-1}$, respectively. The two measurements are identical within errors. A lack of variations suggests that the

Table 1. Additional UVES line identifications.

Ion	λ^a (\AA)	E.W. (m \AA)	v_{bary} (km s^{-1})
Fe II	4233.172	7	36.9
Fe II	4923.927	17	36.9
Fe II	5001.959	22	39.5
Fe II	5018.440	21	36.9
Si II	5041.024	131	42.8
Si II	5055.984 ^b	233	44.5
Fe II	5097.271	12	40.9
Fe II	5100.727	27	38.8
Fe II	5169.033	26	36.8
Fe II	5227.481	17	42.4
Fe II	5260.260	20	40.8

^a Continued from Vennes, Kawka, & Németh (2010a).

^b Blended with Si II $\lambda 5056.317$.

DA white dwarf is not in a close binary system. The average of the two measurements is $\bar{v}_{\text{H}\alpha} = 37.2 \pm 0.6 \text{ km s}^{-1}$.

Table 1 updates the spectral line identifications presented in Vennes, Kawka, & Németh (2010a). A set of nine Fe II lines were observed allowing us to improve our earlier iron abundance measurement. Two strong Si II lines are added to our list, but their line velocities deviate significantly from the rest velocity, set by H α , by 6 and 7 km s^{-1} . A closer examination of other Si II lines observed at epoch 1 also reveals similar radial velocity shifts that shall be investigated in Section 3.3.1. The sulfur lines S II $\lambda 5014.069$, $\lambda 5032.447$, and $\lambda 5432.815\text{\AA}$ were not detected.

3 ANALYSIS AND DISCUSSION

We adopted the model atmosphere analysis of Vennes, Kawka, & Németh (2010a) that was based on non-LTE calculations made with TLUSTY-SYNSPEC (Hubeny & Lanz 1995; Lanz & Hubeny 1995). All models were computed at $T_{\text{eff}} = 20890 \text{ K}$ and $\log g = 7.90$. Vennes, Kawka, & Németh (2010a) found the difference between the best-fitting ($T_{\text{eff}}, \log g$) to the Balmer line series using non-LTE heavy-element blanketed model atmospheres and the best-fitting solution using pure-hydrogen LTE models to be within statistical errors ($\Delta T_{\text{eff}} = +120 \text{ K}$, $\Delta \log g = -.04$). Heavy elements contribute less than 0.1% of the total electron density and their combined opacities are relatively modest in this range of effective temperatures compared to the strong Lyman and Balmer lines and continua.

The model atmosphere structures and synthetic spectra employed in the line profile analysis were computed assuming non-LTE, and with varying abundances of oxygen, magnesium, silicon, calcium and iron. The spectral syntheses are computed with different atomic data sets described below (Section 3.1). Also, we computed spectral syntheses with depth-dependent trace element abundances that were prescribed by diffusion theory (Section 3.2). Finally, we determine the extent of non-LTE effects in the atmosphere of GALEX J1931+0117 by comparing our non-LTE analysis to LTE results (Section 3.3.2).

Table 2. Si II oscillator strengths (f_{ij}).

λ_0 (Å)	CD23 ^a	NIST	Theory ^b	Exp. ^c
3853.665	0.0076	0.0114	0.0090	0.0131±0.0014
3856.018	0.0462	0.0654	0.0535	0.073±0.011
3862.595	0.0381	0.0437	0.0445	0.039±0.007
4128.054	0.518	0.571	0.600	0.57±0.18
4130.872	0.025	0.0275	0.0285	...
4130.894	0.499	0.594	0.570	0.6±0.2
5041.024	0.977	0.534	0.765	0.53±0.09
5055.984	0.979	0.834	0.690	0.83±0.16
5056.317	0.109	0.0805	0.0768	...
5957.559	0.250	0.298	0.233	...
5978.930	0.252	0.303	0.233	...
6347.109	0.991	0.705	0.745	0.66±0.11
6371.371	0.497	0.414	0.373	0.46±0.08

^a Compiled by Kurucz & Bell (1995).

^b Artru et al. (1981).

^c Matheron et al. (2001).

3.1 Atomic data

Our original spectral syntheses were computed with the line list available on the CD-ROM No. 23 of Kurucz & Bell (1995)¹. For each ion, we now compare the oscillator strengths (f_{ij}) and Stark line broadening parameters (Γ) listed by Kurucz & Bell (1995) to the best available theoretical and experimental data. Data on line oscillator strengths are also available at the National Institute of Standards and Technology (NIST).²

We noted that the isotopic shift in the $^{26-24}\text{Mg II } \lambda 2798$ doublet is only $+0.85 \text{ km s}^{-1}$ (Drullinger, Wineland, & Bergquist 1980) and, therefore, we do not expect observable effects on the $\text{Mg II } \lambda 4481$ doublet in 6 km s^{-1} -resolution spectra. Similarly, other isotopic shifts (e.g., $^{30}\text{Si}/^{28}\text{Si}$) may be neglected in the present study (see Berengut, Dzuba, & Flambaum 2003).

3.1.1 Si II

The rich silicon line spectrum in GALEX J1931+0117 prompted a detailed review of available data. Table 2 lists and compares f_{ij} from popular data compilations (CD23 and NIST) to homogeneous theoretical or experimental data sets. We noted considerable variations in Si II oscillator strengths, in particular in the $\lambda 3862$ triplet and in $\lambda 5041.024$. Discrepancies of the order of 40 to 50% would affect individual abundance measurements in equal measures. For example, the ratio of CD23 data to experimental f_{ij} values is 1.06 but varies with a standard deviation $\sigma = 38\%$ while the NIST data that are largely based on the experimental values vary by only 8% with an average ratio of 0.98, and the theoretical data (Artru et al. 1981) vary by 23% with an average ratio of 0.98. The adoption of one data set over another will not have a large effect on the average abundance, but individual line measurements are less reliable.

¹ CD23, accessed at <http://www.cfa.harvard.edu/amp/ampdata/kurucz23/> (Kurucz & Bell 1995).

² Accessed at <http://www.nist.gov/physlab/data/asd.cfm>.

Table 3. Si II Stark widths (FWHM) and shifts.

λ_0 (Å)	CD23 ^a	Theory ^b	Experiments ^c	
	$2w_e$ (Å)	$2w_e$ (Å)	$2w_e$ (Å)	d_e (Å)
3853.665	0.97	0.42	0.52±0.17	-0.17±0.05
3856.018	0.97	0.42	0.50±0.11	-0.05±0.01
3862.595	0.97	0.42	0.50±0.13	-0.03±0.01
4128.054	1.22	0.96	0.97±0.15	-0.23±0.03
4130.894	1.22	0.96	1.01±0.11	-0.20±0.02
5041.024	2.69	1.95	2.54±0.18	+0.86±0.06
5055.984	2.71	1.95	2.58±0.34	+0.93±0.12
5957.559	2.32	2.27	2.72±0.54	+1.32±0.26
5978.930	2.33	2.27	2.78±0.42	+1.19±0.18
6347.109	1.95	1.44	1.13±0.26	-0.31±0.07
6371.371	1.97	1.44	0.99±0.25	-0.29±0.07

^a Compiled by Kurucz & Bell (1995).

^b Lanz, Dimitrijevic, & Artru (1988) calculated at $n_e = 10^{17} \text{ cm}^{-3}$ and $T = 20 \times 10^3 \text{ K}$.

^c At $n_e = 10^{17} \text{ cm}^{-3}$ and $T = 16 - 20 \times 10^3 \text{ K}$ (González et al. 2002; Lesage 2009).

Strong saturated lines are sensitive to line broadening parameters. Table 3 lists full-width at half-maximum (FWHM $\equiv 2w$) Stark widths and shifts due to electron impacts for strong Si II optical lines. Kurucz & Bell (1995) tabulate the circular frequency per electron Γ that we converted into the FWHM at $n_e = 10^{17} \text{ cm}^{-3}$ using the formula:

$$2w = \frac{1}{2\pi} \Gamma \frac{\lambda^2}{c} n_e, \quad (1)$$

where c is the speed of light. Lanz, Dimitrijevic, & Artru (1988) tabulates FWHM values for electron and proton impacts separately. For most lines the proton contribution to the total width is $\approx 10\%$ up to 15%. The FWHM from Kurucz & Bell (1995) are on average 43% larger than the experimental values with a standard deviation of 44% while the values from Lanz, Dimitrijevic, & Artru (1988) are only 6% lower than the experimental values with a standard deviation of 21%.

The excellent agreement between Lanz, Dimitrijevic, & Artru (1988) and the experiments prompted us to explore two options in computing detailed silicon line spectra. In option 1 we adopted the silicon oscillator strengths from Artru et al. (1981) and the line broadening parameters for electrons and protons from Lanz, Dimitrijevic, & Artru (1988). The line broadening parameters are tabulated at 5, 10, 20, and $40 \times 10^3 \text{ K}$ with estimated uncertainties of less than 20% at $n_e = 10^{17} \text{ cm}^{-3}$ (or a depth $\tau_R \approx 2$ in the atmosphere). Also, the effect of Stark shifts are included using the experimental data of González et al. (2002) although we have no information on the scaling of d_e with temperature or on the magnitude of Stark shifts due to ions (protons in this case). The effect of Stark shifts is apparent in radial velocity measurements of the Si II $\lambda\lambda 5041-5055$ and $\lambda\lambda 5967-5978$ multiplets (see Table 1 and Vennes, Kawka, & Németh 2010a). In option 2, we employed the data (f_{ij} and Γ) compiled by Kurucz & Bell (1995), and neglected the effect of Stark shifts.

Table 4. Mg II Stark widths (FWHM) and shifts.

λ_0 (Å)	Γ Est. ^a	Theory ^b		Experiments ^c	
	$2w_e$ (Å)	$2w_e$ (Å)	d_e (Å)	$2w_e$ (Å)	d_e (Å)
4481.126	1.09	2.50	-0.0883	2.95	-0.085

^a Estimated using the classical formula and $n_{\text{eff}} = 4$.

^b Dimitrijević & Sahal-Bréchet (1995) calculated at $n_e = 1.35 \times 10^{17} \text{ cm}^{-3}$ and $T = 16.9 \times 10^3 \text{ K}$.

^c Measured at $n_e = 1.35 \times 10^{17} \text{ cm}^{-3}$ and $T = 16.9 \times 10^3 \text{ K}$ (Djenize, Srećković, & Bukvić 2005; Lesage 2009).

3.1.2 Mg II

Unlike silicon, the magnesium abundance measurement is based on a single doublet. The red Mg II $\lambda 7989$ multiplet shows evidence of Stark shifts (Vennes, Kawka, & Németh 2010a) although the spectrum is particularly noisy in the vicinity of the multiplet. On the other hand, the strong Mg II $\lambda 4481$ doublet is well exposed. Because of its strength, the line profile is particularly sensitive to broadening parameters, although quoted oscillator strength values are consistent (NIST and Kurucz & Bell 1995) within $\lesssim 2\%$.

The compilation of Kurucz & Bell (1995) does not provide a Stark width for the Mg II $\lambda 4481$ doublet which is then estimated in SYNSPEC using the formula (Castelli 2005)

$$\Gamma = 10^{-8} n_{\text{eff}}^5, \quad (2)$$

where Γ is expressed in $\text{rad s}^{-1} \text{ cm}^{-3}$ and n_{eff} is the effective quantum number in the hydrogenic approximation

$$n_{\text{eff}}^2 = (Z + 1)^2 \frac{13.595}{E_i}, \quad (3)$$

where E_i is the ionization energy (eV) of the upper level of the transition and Z is the ionic charge of the trace element. The Γ value is then converted into the FWHM $2w$. Table 4 shows that theoretical and experimental values of the widths and shifts due to electrons are in agreement but that the estimated width using the classical formula is in error. The Stark shift due to electrons compares well with experiments (see Lesage 2009), although the shift due to protons is predicted to dominate (Dimitrijević & Sahal-Bréchet 1995). Incidentally, Dimitrijević & Sahal-Bréchet (1995) also predict a pressure shift in the Mg II $\lambda 7989$ multiplet of opposite sign and a factor of ≈ 8 larger than in the Mg II $\lambda 4481$ doublet, in qualitative agreement with observations reported here and by Vennes, Kawka, & Németh (2010a).

In step with our investigation of silicon lines, we also developed two options for the analysis of the Mg II $\lambda 4481$ doublet. In option 1 we adopted the NIST oscillator strengths and the line broadening and shift parameters (proton and electron) from Dimitrijević & Sahal-Bréchet (1995). In option 2, we adopted the oscillator strengths from Kurucz & Bell (1995) and the classical line broadening parameter while neglecting pressure shifts.

3.1.3 Ca II

Table 5 compares theoretical and experimental results for the Ca II $\lambda 3933$ resonance line. Stark widths from various sources including Kurucz & Bell (1995) are in

Table 5. Ca II Stark widths (FWHM) and shifts.

λ_0 (Å)	CD23 ^a	Theory ^b		Experiments ^c	
	$2w_e$ (Å)	$2w_e$ (Å)	d_e (Å)	$2w_e$ (Å)	d_e (Å)
3933.663	0.248	0.300	-0.048	0.286	-0.14

^a Compiled by Kurucz & Bell (1995) and accessed at <http://www.cfa.harvard.edu/amp/ampdata/kurucz23/sekur.html>.

^b Dimitrijević & Sahal-Bréchet (1992) calculated at $n_e = 1.76 \times 10^{17} \text{ cm}^{-3}$ and $T = 43 \times 10^3 \text{ K}$.

^c At $n_e = 1.76 \times 10^{17} \text{ cm}^{-3}$ and $T = 43.0 \times 10^3 \text{ K}$ (Srećković & Djenize 1993).

agreement although the pressure shifts calculated by Dimitrijević & Sahal-Bréchet (1992) are a factor of 3 smaller than measured (Srećković & Djenize 1993). Because the measured Ca II $\lambda 3933$ shift is relatively small (see Vennes, Kawka, & Németh 2010a) it may not be measurable in our spectra and the lack of accuracy in these parameters would not affect the abundance and radial velocity analysis.

As part of option 1 we adopt the theoretical broadening and shift parameters of Dimitrijević & Sahal-Bréchet (1992) and in option 2 we adopt again the compilation of Kurucz & Bell (1995) without pressure shifts.

3.1.4 O I and Fe II

The analysis of weak spectral lines is sensitive to the assumed oscillator strengths but it is less sensitive to broadening parameters, and we will not distinguish the two options.

The O I $\lambda 7773$ oscillator strengths tabulated by Kurucz & Bell (1995) and NIST differ by $\approx 10\%$ which implies a minimum uncertainty in oxygen abundance measurements of the same order. Ben Nessib, Lakhdar, & Sahal-Bréchet (1996) compared calculated O I Stark width to Griem (1974) and to experiments. They found excellent agreement between their calculations and the experimental values although they do not provide data for the O I $\lambda 7773$ multiplet. The Stark width tabulated by Griem (1974) and Kurucz & Bell (1995) agree to within a few percent at $T = 20000$ appropriate for our analysis. We adopted the oscillator strengths and Stark widths tabulated by Kurucz & Bell (1995).

Five of the Fe II lines detected in GALEX J1931+0117 are listed at NIST while atomic data for all lines are listed by Kurucz & Bell (1995). In this case, we adopted the oscillator strengths and Stark widths tabulated by Kurucz & Bell (1995).

3.2 Diffusion in white dwarf atmospheres

A tenet of the accretion-diffusion scenario is that photospheric abundances reach a steady-state level in the line-forming region. The abundance gradient is assumed to be zero in convective layers, but it is a function of the diffusion time scale in radiative layers as in the case of GALEX J1931+0117.

Assuming accretion steady-state the mass-continuity equation may be written as

$$c_2 \equiv \frac{n_2}{n_1} = \dot{M}_2 \frac{1}{4\pi R^2} \frac{1}{A_2} \frac{\tau_{1,2}}{m}, \quad (4)$$

where c_2 is the abundance of element “2” relative to the main constituent “1”, \dot{M}_2 is the mass accretion rate of element “2” (g s^{-1}), R is the stellar radius (cm), A_2 is the atomic weight of element “2” (a.m.u),

$$\tau_{1,2} = m/(\rho v_{1,2}) \quad (5)$$

is the diffusion time scale of element “2” (s), m and ρ are the mass loading (g cm^{-2}) and density (g cm^{-3}) in the atmosphere, and $v_{1,2}$ is the diffusion velocity (cm s^{-1}) given by the diffusion equation. Assuming that element “1” is fully ionized hydrogen ($A_1 = 1$, $Z_1 = 1$) and that $c_2 \ll 1$, then the diffusion equation (see Vennes et al. 1988) simplifies to

$$v_{1,2} = D_{1,2} \left(-\frac{1}{c_2} \frac{dc_2}{dr} + (1 - A_2) \frac{m_p g}{kT} + A_2 \frac{m_p g_r}{kT} \right), \quad (6)$$

where $D_{1,2}$ is the diffusion coefficient of trace element “2” relative to the main constituent (see Vennes, Kawka, & Németh 2010b).

The first term on the right-hand side is the actual abundance gradient. We show in Section 3.3.3 that c_2 is a slowly varying function of density, $c_2 \propto \rho^\alpha$ and $|\alpha| \lesssim 0.5$, therefore

$$\left| \frac{1}{c_2} \frac{dc_2}{dr} \right| \lesssim -\frac{1}{\rho} \frac{d\rho}{dr} = \frac{d\rho}{dm}, \quad (7)$$

where $dm = -\rho dr$. The second term on the right-hand side of the diffusion equation is proportional to the surface gravity g and the last term is proportional to the radiative acceleration g_r . Employing the run of density ρ and temperature T as a function of mass loading m in a model atmosphere appropriate for GALEX J1931+0117, it can be shown that gravitational settling acts unimpeded as long as $c_2 \ll 1$, i.e., that

$$\left| \frac{d\rho}{dm} \right| \ll \left| (1 - A_2) \frac{m_p g}{kT} \right|. \quad (8)$$

The abundance gradient term is $\lesssim 2\%$ of the gravity term and does not effectively counteract the gravitational pull. Similarly, radiative forces (Chayer, Fontaine, & Wesemael 1995; Chayer et al. 1995) are relatively weak at $T_{\text{eff}} \approx 20 \times 10^3 \text{K}$ and cannot raise the abundances to levels observed in GALEX J1931+0117. The silicon abundance potentially supported by radiation is at least 3.5 orders of magnitude below the observed abundance, and the radiative forces on oxygen, magnesium, calcium, and iron are negligible.

In summary, unless a diffusion steady-state cannot be reached, the vertical abundance distribution in the atmosphere of an accreting white dwarf follows a relation of the form $c_2 \propto \tau_{1,2}/m$ and may depart significantly from a homogeneous distribution. Longitudinal homogeneity is assumed although abundance spots may in principle occur.

3.3 Line profile analysis

Detailed line profiles are computed and convolved to the instrumental resolution ($R \approx 46000$). The separate routines were introduced into the spectral synthesis code to treat Stark shifts self-consistently. The Voigt profiles, that already include a treatment of Doppler width and damping functions ($\Gamma_{\text{nat}} + \Gamma_{\text{Stark}}$) have been modified to include the effect of Stark shifts. The line centre is shifted linearly with electronic

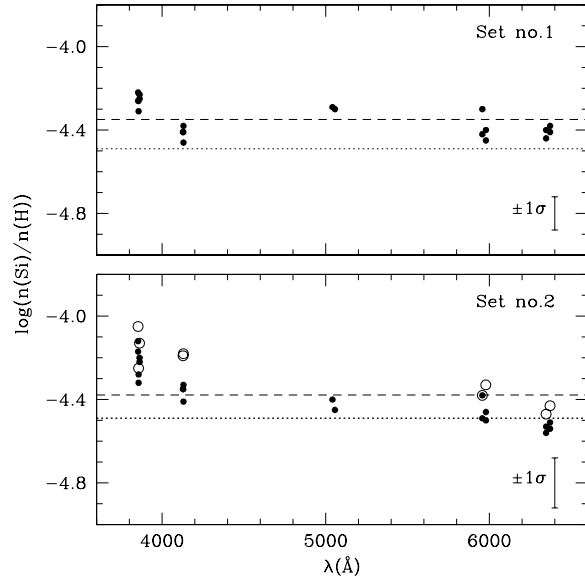


Figure 1. Abundances measured in LTE with individual lines and using two separate atomic data sets. Set number 1 employs line broadening calculations of Lanz, Dimitrijevic, & Artru (1988) and oscillator strengths from Artru et al. (1981) and includes the effect of Stark shifts. Set number 2 employs data compiled by Kurucz & Bell (1995) but excludes Stark Shifts. Twenty abundance measurements (full circles) with set number 1 are shown in the upper panel, while the same abundance measurements using set number 2 are shown in the lower panel along with the non-LTE measurements (open circles) collected by Vennes, Kawka, & Németh (2010a) and showing the extent of non-LTE effects on the silicon abundance measurements. Solar abundance ($\log n(\text{Si})/n(\text{H})_{\odot} = -4.49$) is shown with dotted lines (Asplund, Grevesse, & Sauval 2005) and the measured averages are shown with dashed lines. Standard deviations ($\pm 1\sigma$) for each data set are shown in the lower right corner (see text).

and proton density and proportionally to the Stark shift d tabulated at a reference density. Table 6 lists the revised abundances.

3.3.1 Line broadening and pressure shift

In the present analysis we assume both longitudinal and vertical abundance uniformity. The lack of abundance variations between two observation epochs favours a uniform spread of trace elements across the surface although additional observations are required to rule out a mere coincidence in rotational phases. Figure 1 shows abundance measurements obtained for nine Si II spectral lines in 20 separate measurements and Figure 2 shows sample line profile fits.

The revised silicon abundance is -0.05 dex (or 10%) lower than estimated by Vennes, Kawka, & Németh (2010a) mainly because of the additional lines included in the analysis. In fact, the abundance measurements obtained assuming option 1 were on average 7% larger than with option 2. However, as proposed in option 1, adopting the silicon oscillator strengths and line-broadening parameters from Lanz, Dimitrijevic, & Artru (1988) and Artru et al. (1981), respectively, reduced the scatter in abundance measure-

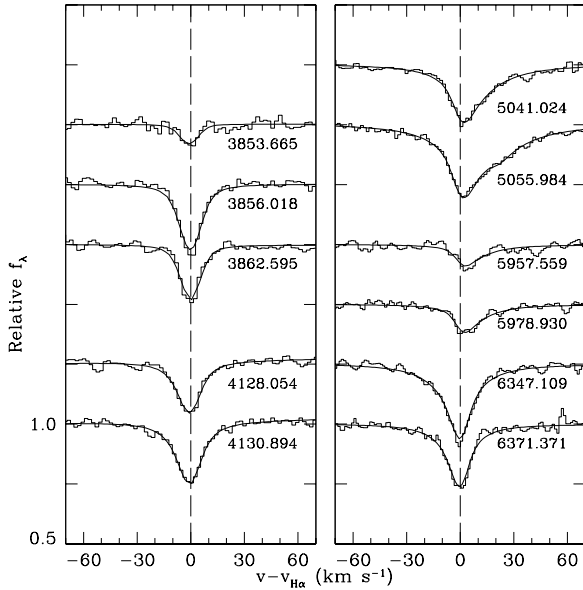


Figure 2. Line profile fits of spectra obtained at epoch 2 and corresponding to abundances depicted in the top panel of Figure 1.

ments based on 20 separate measurements. The scatter in abundance measurements obtained with option 1 was $\sigma = 0.08$ while the scatter obtained with option 2 was larger, $\sigma = 0.13$, while the measurements showed a definite wavelength-dependent trend (Fig. 1).

Moreover, the inclusion of Stark shifts in line profile modelling reduced the scatter in Si II line velocity measurements. The standard deviation of the measurements is $\sigma_v = 2.8$ without shifts down to $\sigma_v = 0.9 \text{ km s}^{-1}$ with Stark shifts included. The average line velocity is $\bar{v} = -0.8$ relative to $v_{H\alpha} = 37.2 \text{ km s}^{-1}$ without Stark shifts and 0.0 km s^{-1} with Stark shifts included. The modelling of the spectral lines with the largest expected Stark shifts has been considerably improved by taking this effect into account (Fig. 2). Figure 3 compares Si II line profiles computed with and without Stark shifts to the observed spectra. The zero velocity is set by the H α line core ($+37.2 \text{ km s}^{-1}$). The line asymmetry in $\lambda 5055$ is due in part to the presence of a weaker Si II line over the extended red wing, but the asymmetric profile in $\lambda 5041$ is entirely due to the Stark shift. The velocity discrepancy notable for these two lines is entirely resolved using Stark shifted profiles.

The calcium abundance was revised slightly down by -0.06 dex (or 14%) mainly because of a small increase in the adopted Stark width. The effect of pressure shift was not noticeable. We estimated the error on the abundance measurements by assuming an uncertainty of 25% on the broadening parameter. The corresponding uncertainty on the abundance is 0.05 dex or 10%.

Our revised magnesium abundance is significantly lower than originally estimated by Vennes, Kawka, & Németh (2010a) entirely because of an upward revision of the Stark width by a factor of two in better agreement with experimental measurements (Table 4). We also estimated the abundance error assuming a 25% uncertainty, i.e., at least the difference between theory and experiments, on the broaden-

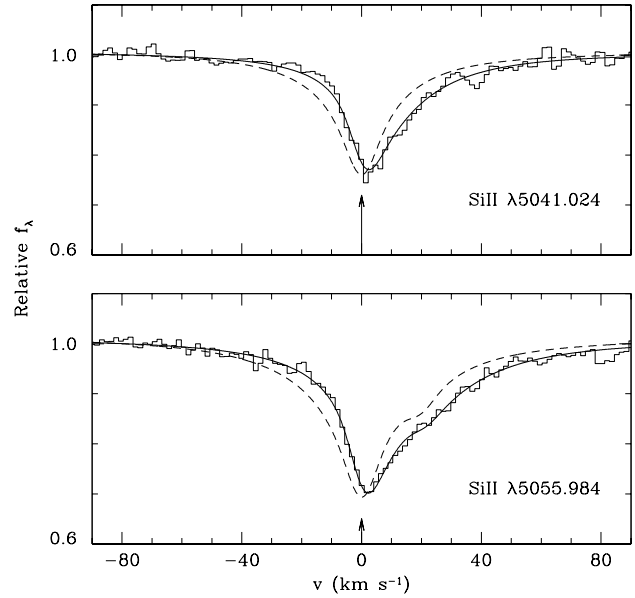


Figure 3. Spectra obtained at epoch 2 are fitted with model line profiles including Stark shifts (full lines) or excluding the effect (dashed lines). The velocity shift in the observed line profiles is well reproduced by models including Stark shifts.

ing parameter. The corresponding uncertainty on the abundance is 0.07 dex or 15%.

The iron abundance, now based on nine separate line measurements, is, within errors, identical to the original estimate. The error was set to the standard deviation of the set of measurements. The procedure adequately propagates uncertainties in broadening parameters and oscillator strengths. However, variations of 25% on the Stark width had no effect on the line equivalent widths. Similarly, the oxygen abundance is identical to the original estimate, and the error was set to the corresponding uncertainty in oscillator strengths (10%). Variations in the Stark width had no effect on the equivalent widths because weak lines such as Fe II and O I lie on the linear part of the curve-of-growth and are insensitive to broadening parameters unlike strong Mg II, Si II, or Ca II lines.

3.3.2 Non-LTE effects on abundance measurements

We measured the abundances using the grid of LTE spectra and compared them to the non-LTE results. We found that non-LTE effects are the largest in highly-excited Si II lines. The average non-LTE shift on abundance measurements is

$$\Delta \log \text{Si}/\text{H} = \log \text{Si}/\text{H}_{\text{NLTE}} - \log \text{Si}/\text{H}_{\text{LTE}} = +0.08 \pm 0.03$$

The abundance shift is $\approx +0.05$ for spectral lines with the lower levels $3s3p^2(^2D)$ or $3s^24s(^2S)$, and $\approx +0.11$ for highly-excited lines with the lower levels $3s^23d(^2D)$ or $3s^24p(^2P^o)$.

A similar comparison of magnesium, calcium, and iron abundances show that non-LTE effects are small:

$$\Delta \log \text{Mg}/\text{H} = -0.02$$

$$\Delta \log \text{Ca}/\text{H} = -0.02$$

$$\Delta \log \text{Fe}/\text{H} = +0.01$$

Finally, the abundance of oxygen measured with highly-excited multiplet O I λ 7773 is relatively large:

$$\Delta \log \text{O}/\text{H} = -0.13$$

In summary, non-LTE effects are notable in highly-excited lines of non-dominant species such as O I, but are negligible in strong lines of dominant species such as Ca II or Mg II. Highly-excited levels of Si II are also affected.

3.3.3 Effect of abundance gradient on line profiles

We investigated the effect of vertical abundance inhomogeneities in the calculation of a spectral line syntheses. The depth-dependent abundance was calculated by fixing the accretion rate \dot{M} and the stellar radius R and varying the diffusion time-scale $\tau_{1,2}$ as a function of mass loading m as described in Section 3.2. We computed the time-scale and corresponding diffusion velocity following Vennes, Kawka, & Németh (2010a). The effect of neutral species on element-averaged velocities was investigated by excluding them from the diffusion velocity calculations and comparing the resulting abundance profiles.

Figure 4 (left) shows that in the line forming region the abundance ratio $c_2 \equiv n_2/n_1$ can be approximated by $c_2 \propto \rho^\alpha$ where $-0.44 \lesssim \alpha \lesssim 0.54$, or $|\alpha| \lesssim 0.5$. The simulations confirm that, in this context, the abundance gradients are not steep enough to counteract gravity (Section 3.2). The effect of neutral species on element-averaged diffusion velocities are more marked in the cases of carbon and oxygen because of the relatively high C I and O I ionization potentials. In the case of oxygen the assumed location of the photosphere bears heavily of the derived accretion rate and other elements may be affected as well. In order to remedy the situation we computed new emerging line profiles parametrized by a constant accretion rate, i.e., an accretion steady-state, rather than a constant abundance throughout the photosphere. These non-LTE spectral syntheses were calculated by adopting the structure (T, ρ) of the best-fitting *homogeneous* model and introducing the abundance distribution prescribed by Equation 4. The observed spectra were then fitted with the model grid and the accretion rates were measured explicitly.

Table 7 lists measured accretion rates for C, O, Mg, Si, Ca, and Fe. The quoted errors are statistical only and do not include systematic errors in modelling the diffusion flow. Calculated concentrations in the line forming region are inversely proportional to diffusion coefficients and errors would scale accordingly, i.e., an error of 50% on theoretical diffusion coefficients would propagate to calculated concentrations. Figure 4 (left) shows the corresponding abundance profiles. The inferred abundances at three different locations in the photospheres (marked with arrows) are in good agreement with the abundance derived from homogeneous models in the case silicon, and they deviate slightly in the case of magnesium and iron. Figure 4 (right) shows model spectra compared to the observed spectrum at three accretion rates. Although abundance inhomogeneities may affect line profiles, in particular in the relative strength of line core and line wings, a comparison of ultraviolet to optical line strengths may be more revealing, particularly for ultraviolet oxygen lines.

The inferred chemical composition of the accretion flow

Table 6. Revised non-LTE abundances in GALEX J1931+0117.

X	$n(\text{X})/n(\text{H})$	$[\text{X}/\text{H}]^a$
C ^b	$< 7 \times 10^{-5}$	< -0.54
O	$2.4 \pm 0.3 \times 10^{-4}$	-0.28
Mg	$3.8 \pm 0.6 \times 10^{-5}$	0.05
Si	$5.8 \pm 1.0 \times 10^{-5}$	0.25
Ca	$7.7 \pm 0.8 \times 10^{-7}$	-0.42
Fe	$3.7 \pm 0.8 \times 10^{-5}$	0.12

^a $[\text{X}/\text{H}] \equiv \log n(\text{X})/n(\text{H}) - \log n(\text{X})/n(\text{H})_\odot$

^b From Vennes, Kawka, & Németh (2010a).

Table 7. Accretion rates for selected elements.

X	$\log \dot{M}$ (g s ⁻¹)	$[\text{X}/\text{Si}]^a$
C	< 8.0	-0.8
O	9.30 ± 0.05	0.1
Mg	7.75 ± 0.06	-0.5
Si	8.25 ± 0.07	...
Ca	6.39 ± 0.04	-0.9
Fe	8.45 ± 0.09	0.0

^a $[\text{X}/\text{Si}] \equiv \log n(\text{X})/n(\text{Si}) - \log n(\text{X})/n(\text{Si})_\odot$

may be estimated by calculating the abundances relative to silicon

$$\frac{n(\text{X})}{n(\text{Si})}_{\text{flow}} = \frac{\dot{M}(\text{X})}{A(\text{X})} \left(\frac{\dot{M}(\text{Si})}{A(\text{Si})} \right)^{-1}, \quad (9)$$

where X refers to C, O, Mg, Ca, and Fe. Table 7 list the corresponding abundance ratios relative to solar ratios. The results show that oxygen must be supplied in larger proportions that afforded by a solar composition, and that silicon is also supplied in larger proportions than carbon, magnesium, or calcium. Iron is apparently supplied in solar proportions relative to oxygen.

In summary, a line profile analysis parametrized by accretion rates rather than constant abundances reveals an oxygen enrichment in the accretion flow. Diffusion calculations show the dominant effect of neutral species on abundance profiles.

4 DISCUSSION AND CONCLUSIONS

We presented a model atmosphere analysis of the high-metallicity white dwarf GALEX J1931+0117. Based on a critical review of available atomic data, their uncertainties, and their impact on the accuracy of abundance measurements, we revised the abundances presented by Vennes, Kawka, & Németh (2010a). The variations are not significant with the exception of magnesium which is revised downward by a factor of two. The abundance pattern shows that the abundance of magnesium, silicon, and iron is near or above the solar abundance, while the abundance of carbon, oxygen and calcium is below the solar abundance. A line profile analysis performed using vertical abundance distributions obtained by solving the steady-state diffusion equation shows that the accretion flow is rich in oxygen and silicon while it is depleted in other elements. The calculations show that although the oxygen abundance is below so-

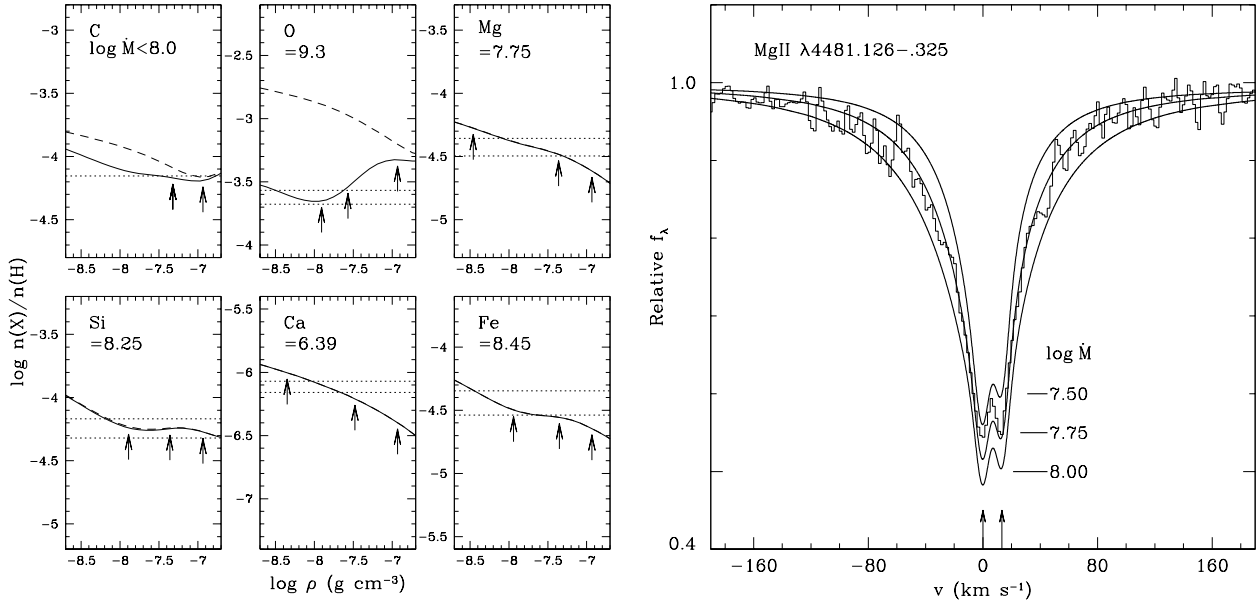


Figure 4. (Left) vertical abundance distribution of elements in the atmosphere of GALEX J1931+0117 computed assuming diffusive steady-state (Section 3.2) and typical accretion rates \dot{M} in g s^{-1} (full lines). The effect of neutral species on element-averaged diffusion velocities and vertical abundance distributions is shown by excluding neutral species from the calculations (dashed lines). The profiles are compared to measured abundances from Table 6 (dotted lines). The locations of optical depth $2/3$ at $\lambda = 1260\text{\AA}$ (rightmost) and in the line wings and center (leftmost) are shown with arrows. (Right) spectrum obtained at epoch 2 (jagged line) compared to model line profiles assuming Mg accretion rates $\dot{M} = 3.2, 5.6,$ and $10 \times 10^7 \text{ g s}^{-1}$.

lar in the line forming region, it must be supplied in larger quantity because of its short diffusion time-scale relative to other elements.

On the other hand, we show that introducing Stark shifts in line profile modelling helped reduce the scatter in line velocity measurements to well within the expected accuracy of the echelle spectra. Investigations of the effect of pressure shifts on radial velocity measurements are relatively rare but their effect have been predicted (e.g., Hammond 1989; Kršljanin & Dimitrijević 1992). A lack of radial velocity variations between two epochs that are 123 days apart also rules out a close binary scenario for the origin of the accreted material. We are left with the possibility that the infrared excess belongs to a warm disc of debris material that accretes onto the white dwarf surface.

The iron abundance in GALEX J1931+0117 is nearly solar (Asplund, Grevesse, & Sauval 2005) and it is comparable to the iron abundance measured in much hotter white dwarfs (Vennes et al. 2006). The resurgence of iron in cooler white dwarfs is also evidence that an external reservoir reached the surface of these objects.

Simulated infrared spectral energy distributions for GALEXJ1931+0117 including a spectral synthesis of the white dwarf added to a warm disc show that the observed distribution (Vennes, Kawka, & Németh 2010a) can be matched by a warm disc (900 K) or a hot disc (1650 K) near sublimation temperature. Necessarily, the inferred dust temperature must be below sublimation temperatures (see Lodders 2003) for the main constituents such as calcium (1659 K), or silicon and magnesium (1354 K). Therefore, the temperature as well as the size and state (gas or solid) of the disc is the result of an adjustment with the host white dwarf

temperature and luminosity. The corresponding disc sizes are $90\Omega_{WD}$ for the hot disc, and, compensating for its reduced emissivity per unit area, $2200\Omega_{WD}$ for the warm disc, where Ω_{WD} is the solid angle subtended by the white dwarf itself. The observed spectral energy distribution extends to the 2MASS measurements in the infrared and measurements at longer wavelengths are required to further constrain the model.

A comparison with other warm DAZ white dwarfs supports these conjectures. The DAZ PG1015+161 ($T_{\text{eff}} = 19300 \text{ K}$, $\log g = 7.9$, $\log \text{Ca}/\text{H} = -5.9$, Koester & Wilken 2006) is similar to GALEX1931+0117 ($T_{\text{eff}} = 20890 \text{ K}$, $\log g = 7.9$, $\log \text{Ca}/\text{H} = -6.1$). Based on JHK and Spitzer observations, Jura, Farihi, & Zuckerman (2007) inferred the presence of a disc with an inner temperature ranging from 800 to 1000 K and emitting area from 700 to 1200 Ω_{WD} . In a similar case, Farihi, Jura, & Zuckerman (2009) inferred the presence of a disc with a blackbody temperature of 1500K around PG1457-086 ($T_{\text{eff}} = 20400 \text{ K}$, $\log g = 8.0$, $\log \text{Ca}/\text{H} = -6.1$). The great diversity in disc emissivity is illustrated by the case of HS0047+1903. Despite having a similar calcium abundance, no evidence of a disc is found in JHK and Spitzer observations (Farihi et al. 2010b).

In conclusion, our analysis of the abundance pattern in GALEXJ1931+0117 and the absence of a close companion, as well as a comparison with other, similar cases such as the DAZ PG1015+161 support the likely presence of a dusty disc around GALEXJ1931+0117.

ACKNOWLEDGMENTS

S.V. and A.K. are supported by GA AV grant numbers IAA300030908 and IAA301630901, respectively, and by GA ĆR grant number P209/10/0967. A.K. also acknowledges support from the Centre for Theoretical Astrophysics (LC06014). We thank M. Kilic for useful discussions and the referee D. Homeier for helpful comments.

REFERENCES

- Artru M. C., Praderie F., Jamar C., Petrini D., 1981, *A&AS*, 44, 171
- Asplund M., Grevesse N., Sauval A. J., 2005, *ASPC*, 336, 25
- Ben Nessib N., Lakhdar Z. B., Sahal-Br  chot S., 1996, *PhysS*, 54, 608
- Berengut J. C., Dzuba V. A., Flambaum V. V., 2003, *PhRvA*, 68, 022502
- Castelli F., 2005, *Mem. S.A.It. Suppl.*, 8, 44
- Chayer P., Fontaine G., Wesemael F., 1995, *ApJS*, 99, 189
- Chayer P., Vennes S., Pradhan A. K., Thejll P., Beauchamp A., Fontaine G., Wesemael F., 1995, *ApJ*, 454, 429
- Debes J. H., 2006, *ApJ*, 652, 636
- Dimitrijevi   M. S., Sahal-Br  chot S., 1992, *Bulletin Astronomique de Belgrade*, 145, 83
- Dimitrijevi   M. S., Sahal-Br  chot S., 1995, *Bulletin Astronomique de Belgrade*, 151, 101
- Djeni  ze S., Sre  kovi   A., Bukvi   S., 2005, *JaJAP*, 44, 1450
- Drullinger R. E., Wineland D. J., Bergquist J. C., 1980, *ApPhy*, 22, 365
- Dupuis J., Fontaine G., Wesemael F., 1993, *ApJS*, 87, 345
- Dupuis J., Chayer P., H  nault-Brunet V., Vennes S., Kruk J. W., 2009a, *AIPC*, 1135, 329
- Dupuis J., H  nault-Brunet V., Chayer P., Vennes S., Kruk J. W., 2009b, *JPhCS*, 172, 012050
- Farihi J., Barstow M. A., Redfield S., Dufour P., Hambly N. C., 2010a, *MNRAS*, 404, 2123
- Farihi J., Jura M., Lee J.-E., Zuckerman B., 2010b, *ApJ*, 714, 1386
- Farihi J., Jura M., Zuckerman B., 2009, *ApJ*, 694, 805
- Farihi J., Zuckerman B., Becklin E. E., 2008, *ApJ*, 674, 431
- Fontaine G., Michaud G., 1979, *ApJ*, 231, 826
- G  nsicke B. T., Marsh T. R., Southworth J., 2007, *MNRAS*, 380, L35
- G  nsicke B. T., Marsh T. R., Southworth J., Rebassa-Mansergas A., 2006, *Sci*, 314, 1908
- Gonz  lez V. R., Aparicio J. A., del Val J. A., Mar S., 2002, *JPhB*, 35, 3557
- Graham J. R., Matthews K., Neugebauer G., Soifer B. T., 1990, *ApJ*, 357, 216
- Griem H. R., 1974, *Spectral line broadening by plasmas* (Pure and Applied Physics Volume 39). Academic Press, Inc, New York
- Hammond G. L., 1989, *LNP*, 328, 346
- Holberg J. B., Barstow M. A., Green E. M., 1997, *ApJ*, 474, L127
- Hubeny I., Lanz T., 1995, *ApJ*, 439, 875
- Jura M., Farihi J., Zuckerman B., 2007, *ApJ*, 663, 1285
- Kawka A., Vennes S., Dupuis J., Chayer P., Lanz T., 2008, *ApJ*, 675, 1518
- Kilic M., von Hippel T., Leggett S. K., Winget D. E., 2006, *ApJ*, 646, 474
- Koester D., 2009, *A&A*, 498, 517
- Koester D., Rollenhagen K., Napiwotzki R., Voss B., Christlieb N., Homeier D., Reimers D., 2005, *A&A*, 432, 1025
- Koester D., Wilken D., 2006, *A&A*, 453, 1051
- Kr  sljanin V., Dimitrijevi   M. S., 1992, *LNP*, 401, 371
- Kurucz R., Bell B., 1995, *Atomic Line Data Kurucz CD-ROM No. 23*. Smithsonian Astrophysical Observatory, Cambridge, MA
- Lanz T., Dimitrijevic M. S., Artru M.-C., 1988, *A&A*, 192, 249
- Lanz T., Hubeny I., 1995, *ApJ*, 439, 905
- Lesage A., 2009, *NewAR*, 52, 471
- Lodders K., 2003, *ApJ*, 591, 1220
- Matheron P., Escarguel A., Redon R., Lesage A., Richou J., 2001, *JQSRT*, 69, 535
- Sre  kovi   A., Djeni  ze S., 1993, *Bulletin Astronomique de Belgrade*, 148, 7
- Vennes S., Chayer P., Dupuis J., Lanz T., 2006, *ApJ*, 652, 1554
- Vennes S., Kawka A., N  meth P., 2010a, *MNRAS*, 404, L40
- Vennes S., Kawka A., N  meth P., 2010b, in Schuh, S., Heber, U., Drechsel, H., eds, *Planetary Systems beyond the Main Sequence*, AIP, in press (arXiv:1012.2644)
- Vennes S., Pelletier C., Fontaine G., Wesemael F., 1988, *ApJ*, 331, 876
- Zuckerman B., Koester D., Reid I. N., H  nsch M., 2003, *ApJ*, 596, 477